Title
Tunnel-FET Switching Is Governed by Non-Lorentzian Spectral Line Shape

Journal
Proceedings of the IEEE, 108(8)

ISSN
0018-9219

Authors
Vadlamani, Sri Krishna
Agarwal, Sapan
Limmer, David T
et al.

Publication Date
2020-08-01

DOI
10.1109/jproc.2019.2904011

Peer reviewed

INVITED PAPER

Tunnel-FET Switching Is Governed by Non-Lorentzian Spectral Line Shape

This article provides new insights into fundamental limitations of the tunnel FETs (tFETs) for desirable energy-efficient operations, and how to possibly overcome them.

By SRI KRISHNA VADLAMANI, *Member IEEE*, SAPAN AGARWAL, *Member IEEE*, DAVID T. LIMMER, STEVEN G. LOUIE, FELIX R. FISCHER, AND ELI YABLONOVITCH, *Fellow IEEE*

ABSTRACT | In tunnel field-effect transistors (tFETs), the preferred mechanism for switching occurs by alignment (ON) or misalignment (OFF) of two energy levels or band edges. Unfortunately, energy levels are never perfectly sharp. When a quantum dot interacts with a wire, its energy is broadened. Its actual spectral shape controls the current/voltage response of such transistor switches, from on (aligned) to off (misaligned). The most common model of spectral line shape is the Lorentzian, which falls off as reciprocal energy offset squared. Unfortunately, this is too slow a turnoff, algebraically, to be useful as a transistor switch. Electronic switches generally demand an ON/OFF ratio of at least a million. Steep exponentially falling spectral tails would be needed for rapid off-state switching. This requires a new electronic feature, not previously recognized: narrowband, heavy-effective mass, quantum wire electrical contacts, to the tunneling quantum states. These are a necessity for spectrally sharp switching.

KEYWORDS | Field-effect transistors (FETs); quantum dots; resonant tunneling devices

Manuscript received August 4, 2018; revised January 19, 2019; accepted February 28, 2019. Date of publication April 11, 2019; date of current version July 17, 2020. The work of S. K. Vadlamani, F. R. Fischer, S. G. Louie, and E. Yablonovitch was supported by the National Science Foundation through the Center for Energy Efficient Electronics Science (E^3S) under Award ECCS-0939514. The work of S. G. Louie was also supported in part by the ONR Program Carbon-Based Hierarchically Integrated Synthetic Electronics (CHISEL) under Grant ONR-15-FOA-0011 and in part by NSF under Grant DMR-1508412. The work of S. Agarwal was supported by the Laboratory Directed Research and Development Program at Sandia National Laboratories, a multimission laboratory managed and operated by the National Technology and Engineering Solutions of Sandia, LLC., a wholly owned subsidiary of Honeywell International, Inc., for the U.S. DOE's National Nuclear Security Administration under Contract DE-NA-0003525. This paper describes objective technical results and analysis. Any subjective opinions do not necessarily represent the views of the U.S. Department of Energy or the U.S. Government. The work of D. T. Limmer was supported by the UC Berkeley College of Chemistry. *(Corresponding author: Sri Krishna Vadlamani.)*

S. K. Vadlamani and **E. Yablonovitch** are with the Electrical Engineering and Computer Sciences Department (EECS), University of California at Berkeley, Berkeley, CA 94720 USA (e-mail: srikv@berkeley.edu; eliy@eecs.berkeley.edu).

S. Agarwal was with the Electrical Engineering and Computer Sciences Department (EECS), University of California at Berkeley, Berkeley, CA 94720 USA. He is now with the Sandia National Laboratories, Albuquerque, NM 87185 USA (e-mail: sagarwa@sandia.gov).

D. T. Limmer and **F. R. Fischer** are with the Chemistry Department, University of California at Berkeley, Berkeley, CA 94720 USA (e-mail: dlimmer@berkeley.edu; ffischer@berkeley.edu).

S. G. Louie is with the Physics Department, University of California at Berkeley, Berkeley, CA 94720 USA (e-mail: sglouie@berkeley.edu).

Digital Object Identifier 10.1109/JPROC.2019.2904011

I. EFFECT OF SPECTRAL LINE SHAPE ON tFET SWITCHING

One of the most central problems in physical science is predicting and understanding spectral line shape. A Lorentzian line shape $1/(\Delta\omega^2+(\Gamma/2)^2)$ is often assumed, where $\Delta\omega$ is the spectral shift from its resonant position and Γ is an associated linewidth. However, this form rarely applies in condensed matter physics. In the solid state, the optical spectrum of electronic transitions usually decays exponentially, the so-called Urbach tail [1], $\sim\exp\{\Delta\omega/\Gamma_U\}$, with a characteristic Urbach energy $\hbar\Gamma_U$.

This exponential falloff permits materials to be very transparent in the infrared, as required for long-distance optical communication [2] in glass fibers. If the electronic transitions in the glass had a Lorentzian line shape instead, which falls off slowly as $\sim 1/\Delta\omega^2$, the infrared optical absorption would never quite turn off, and the communication attenuation length would be $\sim$1 m. Lorentzian line shape in glass would be a catastrophe for modern civilization, which relies upon optical fibers for worldwide connectivity.

Despite its importance to telecommunications, there is no physics consensus for a simple, common, origin of

Urbach tail spectra, though many complex physical models have been proposed [3]–[9].

In this paper, we introduce another instance in which an exponentially decaying spectrum is important in technology, namely, the tunnel field-effect transistor (tFET). tFETs are attractive as an alternative to the MOSFET because they are not fundamentally limited by the thermal subthreshold slope limit of 60 mV/dec [10]. tFETs were first conceived of in the late 1970s [11] and several early theoretical proposals and experimental demonstrations followed in the ensuing couple of decades [12]–[16], although none of them exhibited subthermal subthreshold slopes. In the 2000s and the 2010s, a large variety of device structures and material systems under various thermal, stress, and other physical conditions were investigated [17]–[34], and we now have several theoretical proposals, backed by simulations [35]–[41], and experimental demonstrations [42]–[57] of devices with subthreshold slopes either below 60 mV/dec or very close to it. Unfortunately, the theoretical predictions are not confirmed by the device results. For example, the subthermal subthreshold slope is achieved only for a few decades of current or at very low current levels.

At a fundamental level, the exact shape of the spectral line shape, that is, band tails of materials, plays a crucial role in determining the subthreshold slope of tFETs. This is not widely recognized, though some prior work has been done in this regard [58], [59]. In this paper, we study the problem of spectral line shape in tFETs and deduce criteria that are necessary for a tFET to have exponential subthreshold behavior.

In tFETs, there are two mechanisms as follows, which can be exploited to obtain improvements in the subthreshold slope [60].

1) The tunneling distance can be modulated [61]–[63].
2) The energy levels can be aligned or misaligned between the source and drain, sometimes called the energy-filtering mechanism [64], [65].

Tunnel distance modulation is more common, but its response to control signals becomes less steep and more gradual at precisely the higher conductance densities that are actually needed for driving wires in a circuit [66].

Thus, the preferred mechanism for switching occurs by energy filtering, alignment (ON) or misalignment (OFF), of two energy levels or band edges. Nonetheless, energy levels are never perfectly sharp. Their actual spectral shape controls the current/voltage response of such transistor switches, from on (aligned) to off (misaligned).

The ON-state is illustrated in Fig. 1(a) in which a valence band quantum well faces a conduction band quantum well. Tunneling occurs from the highest valence band level to the lowest conduction band level, as illustrated by the green arrow. External electrical contact, to the quantum wells, is illustrated by the resistors R connected to the quantum levels in Fig. 1(a). These are usually tunnel resistors. Off-switching occurs when the two quantum levels are misaligned, as shown in Fig. 1(b). Since the quantum levels have finite linewidth, the switching process is actually gradual, depending on level sharpness. In Fig. 1(b), tunneling occurs over a range of energies, a convolution between the spectral density on one side and the spectral density on the other side. Tunneling between the two spectral tails is illustrated by the red arrow. If the spectral sharpness is insufficient, the current does not turn off.

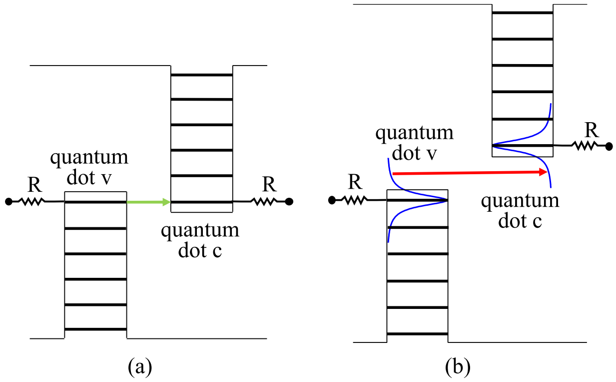

Fig. 1. ***Principle behind the energy-filtering mechanism for tFET. (The gate electrode is not shown.) (a) Topmost valence band energy level of a small area quantum well aligns with the bottom-most conduction band energy level, allowing current to pass (green arrow). Because of device miniaturization, the two respective states are effectively quantum dots. (b) Attempt to switch the device off. Because of the spectral tails of the respective energy levels, current continues to leak from valence to conduction band.***

The most commonly assumed model of spectral line shape is the Lorentzian $S(\Delta\omega) \sim 1/(\Delta\omega^2 + (\Gamma/2)^2)$, which is associated with the familiar time-domain exponential decay of population $\sim\exp\{-\Gamma t\}$. However, away from the line center, Lorentzian line shape falls off as $S(\Delta\omega) \sim 1/\Delta\omega^2$, which is algebraically too slow turnoff to be useful as a transistor switch. Switches generally demand at least 10^6 ON/OFF ratio. Sharper spectral tails are needed.

Fortunately, experimental observations in condensed matter show that the broad spectral tails associated with the Lorentzian line shape are the exception rather than the rule. Line shapes with exponentially falling spectral tails are a necessity for the energy-filtering mechanism in tFETs. In this paper, we will derive the origin of rapidly falling exponential spectral wings[1] $S(\Delta\omega) \sim \exp\{-\Delta\omega/\omega_o\} = \exp\{-2\Delta\omega\tau_p\}$, where $\omega_o = 1/2\tau_p$ is a desired decay constant in the frequency domain. This spectral shape provides the required rapid turnoff mechanism for tFET electrical switches.

Exponential spectral tails can occur in tunneling but may also apply to other spectral line shape phenomena in physics and chemistry. Indeed, exponentially falling spectra are common in condensed matter, but broad Lorentzian spectra are rare.

[1]In the above, band tails means well beyond the central full-width at half-maximum ($\Delta\omega \gg$FWHM).

II. LIFETIME BROADENING OF QUANTUM DOT TO A WIRE CONTACT

We envision the tunnel switch to be nanoscopic, consistent with Moore's law. Thus, there is no loss of generality by considering the lowest energy state of the conduction band shown in Fig. 1 to be an isolated quantum level or dot, and likewise for the highest valence band level acting as a single quantum dot. Our goal is to assign a spectral shape to the individual dots. An empty conduction band quantum dot will accept an electron by tunneling. However, the dot is connected to a wire contact and the electron will leak away, increasing the spectral linewidth by lifetime broadening.

The spectrum $S(\Delta\omega)$ associated with electrical contact to the quantum dot is the Fourier transform of the amplitude decay represented by the projection $\langle\Psi(0)|\Psi(t)\rangle$, of the decayed quantum dot state $|\Psi(t)\rangle$, onto the original filled quantum dot wave function $|\Psi(0)\rangle$. Since we are considering only simple[2] lifetime broadening of the quantum dot, the amplitude as represented by $\langle\Psi(0)|\Psi(t)\rangle$ is positive and decaying to zero. The spectral broadening is the Fourier transform of the wave function correlation function $\mathrm{S}(\omega) = \int_{-\infty}^{\infty}\langle\Psi(0)|\Psi(t)\rangle \mathrm{e}^{-i\omega t}dt$, which simplifies into the cosine transform given by $\mathrm{S}(\omega) = 2\int_0^{\infty}|\langle\Psi(0)|\Psi(t)\rangle|\cos(\omega t)dt$.

Thus, there is a simple Fourier link between the amplitude decay and spectral shape, as illustrated in Fig. 2. For example, the Lorentzian spectral line shape $1/(\Delta\omega^2 + (\Gamma/2)^2)$, the red curve in Fig. 2(b), when subject to an inverse Fourier transform back to the time domain, becomes the classic exponential time decay $\exp(-\Gamma t/2) \equiv \exp(-t/2\tau)$, the red curve in Fig. 2(a). Conversely, exponential tails in the frequency domain result from an initial quadratic (nonexponential) decay in the time domain, as we show now.

In fact, every good quantum mechanics textbook [69] warns that for early times, the quantum amplitude actually falls quadratically $1-t^2/8\tau\tau_p$, far more slowly than the initial linear decay expected from $\exp(-t/2\tau)$, as illustrated by the blue curve in Fig. 2(a). This slow initial quadratic decay in time eventually reverts to the familiar exponential time decay, after a brief induction period $2\tau_p$.

The shape of the early time decay $t/\tau \ll 1$ controls the spectrum at a high spectral shift $\Delta\omega \gg$ FWHM. Early time quadratic decay when transformed back to the frequency domain leads to exponential spectral tails $S(\Delta\omega) \sim \exp\{-2\Delta\omega\tau_p\}$ [the blue curve in Fig. 2(b)] rather than broad Lorentzian spectral tails [the red curve in Fig. 2(b)]. Initial quadratic decay is sufficient to produce exponential tails that provide strong OFF-state switching in tFETs.

To put it succinctly, in our model, lifetime broadening is controlled by two times, τ and τ_p, where $\tau_p \leq \tau$.

[2]Phase-dependent broadening associated with complex amplitude decay and T_2-type broadening will further challenge tFET performance.

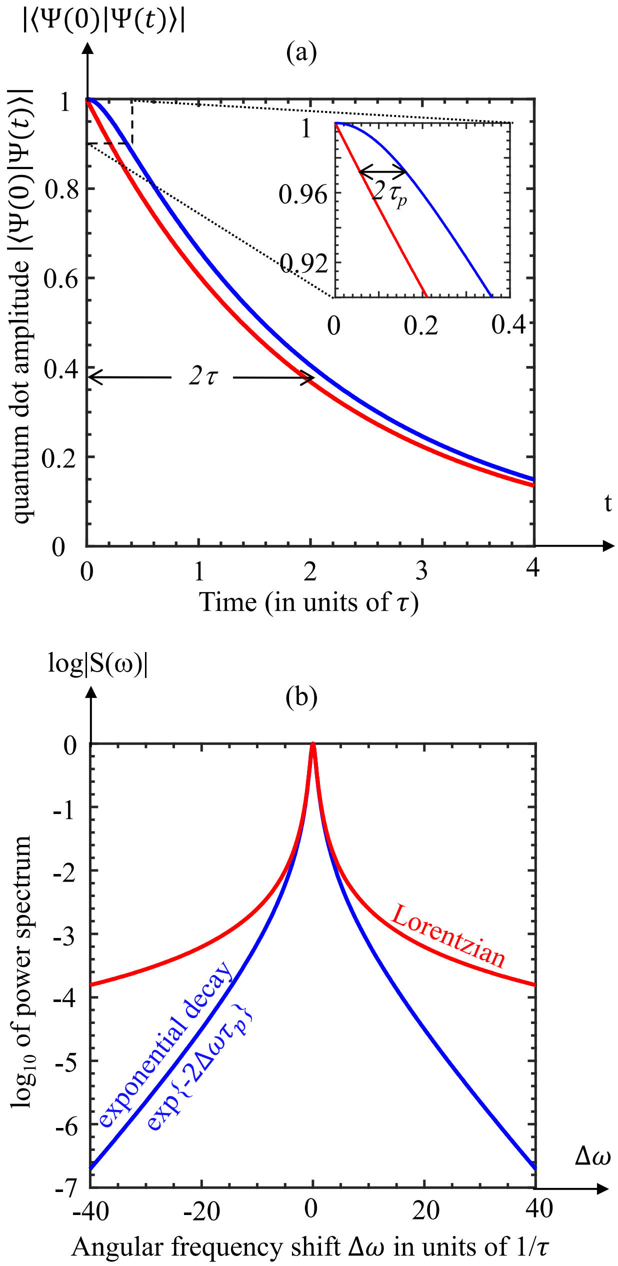

Fig. 2. ***Energy levels are spectrally broadened by the exchange of electrons with the contacts. (a) Time domain. The loss of electrons from a quantum dot causes lifetime broadening. The decay is represented by the projection $|\langle\Psi(0)|\Psi(t)\rangle|$, onto the originally filled quantum state $|\Psi(0)\rangle$. The decay in time can be either exponential from the earliest times (red), or have an initial parabolic decay period $2\tau_p$ (as shown in the inset), before exponentially decaying with a time constant 2τ (blue). (b) Corresponding spectra: a broad Lorentzian (red) and exponential spectral tails (blue).***

The central part of the spectrum, the full-width at half-maximum (FWHM), is controlled by $1/\tau$ and the distant spectral tails fall off exponentially with frequency $1/2\tau_p$.

III. MECHANISM FOR THE INITIAL QUADRATIC TIME DECAY

The simplest model of exponential time decay is Fermi's golden rule approximation for population decay:

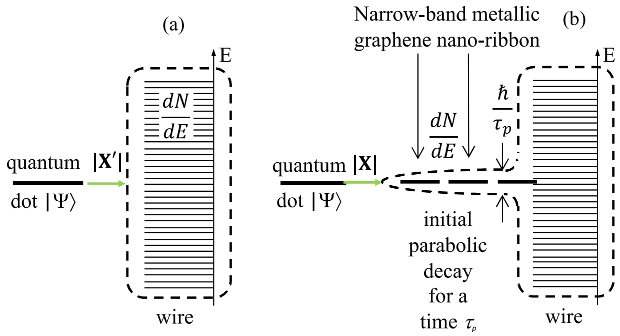

Fig. 3. ***(a) Conventional picture of lifetime broadening due to decay from the quantum dot level $|\Psi\rangle$ to a contact continuum, using Fermi's golden rule. (b) Inserting a narrowband wire between the quantum dot and the contact will ensure that the initial decay of the electron population of the quantum dot is quadratic, leading to exponential line shapes.***

$\Gamma \equiv 1/\tau = (2\pi/\hbar)|\mathbf{X}'|^2(dN/dE)$, as illustrated in Fig. 3(a). This implies the exponential decay of quantum dot amplitude $|\langle\Psi(0)/\Psi(t)\rangle| = \exp(-t/2\tau)$. The corresponding Lorentzian line shape $1/(\Delta\omega^2 + (1/2\tau)^2)$ is incompatible with the required tFET ON/OFF ratio. Implicit in Fermi's golden rule is that the tunneling matrix element $|\mathbf{X}'|$ couples to an infinite range of energy states in the wire, dN/dE. In this case, the exponential $\exp(-t/2\tau)$ begins right at $t = 0$, and we are stuck in the Lorentzian behavior (the red curves in Fig. 2).

By contrast, the blue curves in Fig. 2(b), which contain exponential tails in the frequency domain, can be obtained by truncating to a narrower density of final states dN/dE with a finite bandwidth $E_{\text{narrow-bandwidth}}$ spread over $\pm\hbar/2\tau_p$, as shown in Fig. 3(b). This achieves the initial parabolic decay for a time $2\tau_p$, as indicated in Fig. 2(a). Thus, we would benefit from a mechanism that limits the bandwidth of the density of final states. We must isolate the final state from the wire so that it does not broaden much. At the same time, the current flow must not be restricted. One way of doing this is to introduce a narrowband wire, with a small electron energy bandwidth, between the quantum dot and the actual metal contact, as shown in Fig. 3(b). Having a narrowband final density of states to tunnel into, as opposed to a large bandwidth final density of states, ensures that the decay of electron population in the quantum dot is quadratic for short times. This early time quadratic behavior translates into exponential tails in the energy domain. Despite the heavy effective mass, the narrowband wire, there is no loss in conductivity, which is controlled by the conductance quantum in the ballistic regime.

The narrowband wire that receives electrons from the quantum dot itself has a finite density of states, dN/dE, with bandwidth $\hbar/\tau_p$. Then, an initial parabolic amplitude-induction period $2\tau_p$ for the initial $|\Psi(t)\rangle$ quantum dot decay is guaranteed. This is later followed by the normal exponential quantum dot decay by Fermi's golden rule, $|\langle\Psi(0)|\Psi(t)\rangle| \sim \exp(-t/2\tau)$, as shown by the blue curve in Fig. 2(a), $\tau_p \leq \tau$.

The initial parabolic decay can be explained as follows. The amplitude decay of an electron from the quantum dot in two sequential steps: initially, there is a coherent evolution between the quantum dot state $|\Psi\rangle$ and the state at the tip of the narrowband wire. These oscillate at an angular frequency $2|\mathbf{X}|/\hbar$. This manifests itself initially as a quadratic decay of quantum dot amplitude

$$|\langle\Psi(0)|\Psi(t)\rangle| = \sqrt{1 - (|\mathbf{X}|t/\hbar)^2} = 1 - |X|^2t^2/2\hbar^2.$$

This initial oscillation is terminated at time $t = 2\tau_p$ by the exponential time decay τ, long before even one oscillation is completed, $\tau_p \ll \hbar/|\mathbf{X}|$.

The resulting time decay of the quantum dot amplitude is plotted in blue in Fig. 2(a), with the corresponding lifetime broadened spectrum in blue in Fig. 2(b), for the specific case of $\tau_p = 0.1\tau$.

The value of $1/\tau$ can be calculated by plugging in the value of the final density of states into Fermi's golden rule. The final state is now the tip state of the narrowband wire for which the peak value of the density of states is $dN/dE = 2\tau_p/\pi\hbar$. Hence, the later, exponential portion of the $|\langle\Psi(0)/\Psi(t)\rangle|$ decays as

$$1/\boldsymbol{\tau} = (2\pi/\hbar)|\mathbf{X}|^2(dN/dE) = (2\pi/\hbar)|\mathbf{X}|^2(2_p/\hbar). \quad (1)$$

In summary, the electron population in the quantum dot experiences an initial quadratic decay given by

$$\rho_{\text{dot}}(t) = 1 - (|\mathbf{X}|t/\hbar)^2 \quad (2)$$

for a period of $2\tau_p$ followed by an exponential decay given by

$$\rho_{\text{dot}}(t) = \exp(-t/\tau) = \exp(-(2\pi/\hbar)|\mathbf{X}|^2(2\tau_{\text{p}}/\pi\hbar)t). \quad (3)$$

The short-time and long-time behaviors above can be stitched together using the following fitting function:

$$\rho_{\text{dot}}(t) \sim \exp(b - \sqrt{b^2 + (t/\tau)^2}) \quad (4)$$

where $b = \hbar^2/2(|\mathbf{X}|\tau)^2 = 2\tau_p/\tau$. This function has the correct limits at short and long times and expands in even powers of time only, starting out quadratically at $t = 0$. The blue curves, plotted in Fig. 2, comprise this approximate temporal form $\rho_{\text{dot}}(t) \sim \exp(b - (b^2 + (t/\tau)^2)^{1/2})$, in Fig. 2(a), and its Cosine transform spectrum, in Fig. 2(b). The initial temporal quadratic decay of occupation probability guarantees exponentially falling spectral tails, the main topic of this paper.

As an aside, the physics of a quantum dot coupled to a narrowband wire is analogous to an atom weakly coupled to an electromagnetic cavity with a cavity decay time τ_p. If $\tau_p \ll \hbar/|\mathbf{X}|$, the cavity is very lossy, and we call this weak coupling; if $\tau_p \gg \hbar/|\mathbf{X}|$, a very high-Q cavity, we call it strong coupling. In the optical case, $|\mathbf{X}|$ would be the Rabi matrix element between the excited atom and the electromagnetic cavity. The corresponding weak coupling optical cavity is shown in Fig. 4. The analogy is incomplete, given that in the open optical cavity, the excited atom could directly decay by vertical spontaneous emission, an alternative to cavity loss. The correspondence is reestablished if that external emission is regarded as a weak probe. This suggests that the lifetime broadening of an excited atom, in weak coupling with an electromagnetic cavity, has an exponentially decaying spectral line shape, rather than Lorentzian, which is worth testing.

IV. CURRENT–VOLTAGE CHARACTERISTICS OF THE ENERGY FILTERED tFET

Neglecting the very brief initial quadratic period τ_p, there is a finite mean lifetime τ for an electron to remain on the dot or conversely to jump back to the dot from the narrowband wire. If the quantum dot is occupied, but the narrowband wire states are unoccupied, the maximum current flow is $\sim 2q/\tau$, where the value 2 arises from two possible spin states. If there is a Fermi–Dirac distribution with occupation f_d and Fermi level E_{Fd} on the dot, and corresponding f_w and E_{Fw} on the narrowband wire, the net current is diminished as $(2q/\tau)(f_d - f_w)$, upon allowing for reverse current. For Fermi–Dirac statistics, the difference in occupation is $(f_d - f_w) \sim (E_{Fd} - E_{Fw})/4kT \equiv q\Delta V/4kT$, as given in [71]. Therefore, the current flow $I = (2q/\tau)(q\Delta V/4kT)$ is proportional to voltage difference, and we can define a conductance of the tunnel contact to be $G_{\text{contact}} \equiv (2q/\tau)(q/4kT)$ in the low-voltage regime $\Delta V < 4kT$. By taking account of thermal occupation in this way, a tunneling current can be converted to a conductance. (Using the uncertainty principle inequality, $\hbar/\tau \leq q\Delta V$, G_{contact} is always $\leq q^2/h$, the quantum of conductance, for a single tunneling channel.)

The tFET is built from two quantum dots, as shown in Fig. 5(a), which is a graphene nanoribbon example. As electrons transition from a filled valence band dot to an empty conduction band dot, we can calculate the current and then convert it to conductance. When the energy levels are aligned, the dot–dot peak current can be written by

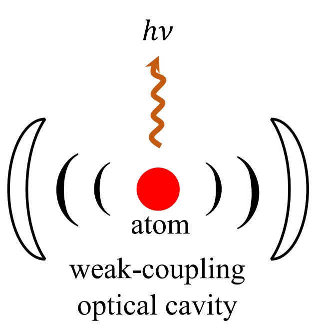

Fig. 4. ***There is an analogy between dot-wire tunneling and an excited atom interacting with a weakly coupled cavity. First, the excitation energy transfers to the cavity. Then, the cavity has electromagnetic losses analogous at a rate 1/τ_p. There needs to be a small side leakage vertically so that the spectrum can be measured. A non-Lorentzian spectrum is predicted, similar to the blue curve in Fig. 2(b).***

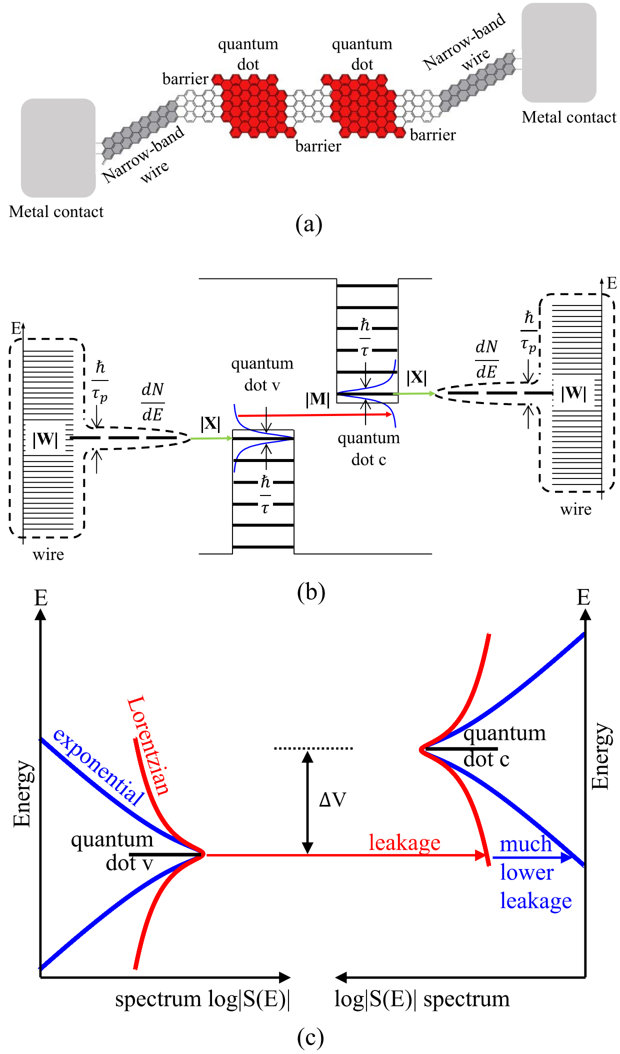

Fig. 5. ***(a) Graphene nanoribbon version of a tFET. (b) Two quantum dots, valence band v, and conduction band c, forming the source and drain, respectively, of a tFET (the gate, which is not shown, electrostatically controls one of the two quantum dots). Because of the misalignment of c and v, the device is switching off, with weak tunneling indicated by the red arrow, and mediated by matrix element $|\mathbf{M}|$. The dots $|\Psi\rangle$ are lifetime broadened, 1/τ, and contact the narrowband wire, by matrix element $|\mathbf{X}|$. (c) Lorentzian spectral tail, red, causes unacceptable leakage in the off-state, while the blue exponential spectral tails fall off rapidly, consistent with the customary metric: "millivolts per decade."***

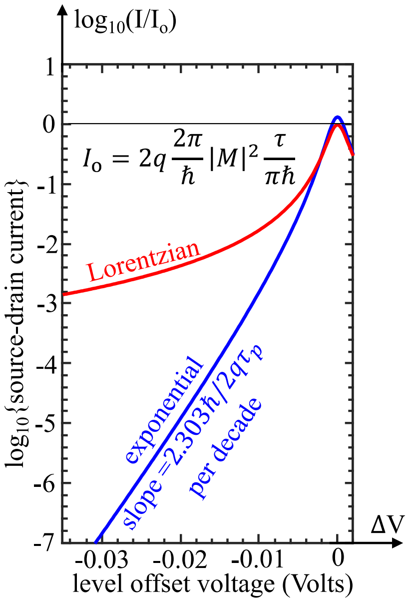

Fig. 6. ***Based on the overlap between valence and conduction band spectral tails, the subthreshold, current-voltage characteristic is shown. The exponential spectral tails produce a leakage that can be characterized in terms of steepness or voltage swing: "millivolts per decade." For this numerical example,*** $(\hbar/(2q\tau_p)) =$ ***2.6 mV,*** $\tau =$ ***500 fsec*** $= 4\tau_p$***, and the steepness*** $2.303\hbar/2q\tau_p =$ ***6 mV/decade. The Lorentzian spectrum has unacceptable leakage. The normalization current*** I_o ***is the on-state current for aligned Lorentzian quantum dots.***

Fermi's golden rule

$$I_{\text{peak}} = 2q\frac{2\pi}{\hbar}|\mathbf{M}|^2\left.\frac{dN}{dE}\right|_c = 2q\frac{2\pi}{\hbar}|\mathbf{M}|^2\frac{2\tau}{\pi\hbar} \tag{5}$$

where $\mathbf{M}$ is the Hamiltonian matrix element between the two quantum dots, $dN/dE|_c$ is the density of states of the empty conduction band dot c, and $\hbar/\tau$ is its energy FWHM associated with the lifetime broadening of the conduction band quantum dot c. There is an extra prefactor 2 to account for tunneling of both electron spins. For $dN/dE|_c$, it is safe to use a normalized Lorentzian line shape: $dN/dE|_c = ((2\tau/\pi\hbar)/(1+4\omega^2\tau^2))$ since the current normalization hardly depends on the band tails at all. In this case, the valence band dot is sharp but the conduction band dot is broadened.

Considering that the initial valence band dot energy level is also broadened, the current equation needs to be modified by averaging over the distribution $dN/dE|_{\text{v}}$ of initial valence band dot state v. The dot–dot peak current when the two density-of-states distributions are aligned is

$$I_{\text{peak}} = 2q\frac{2\pi}{\hbar}|\mathbf{M}|^2\int_{-\infty}^{\infty}\left.\frac{dN}{dE}\right|_{\text{v}}\left.\frac{dN}{dE}\right|_c dE = 2q\frac{2\pi}{\hbar}|\mathbf{M}|^2\frac{\tau}{\pi\hbar}. \tag{6}$$

Surprisingly, averaging over broadened initial states only changes the peak current by half, for the case of both density of states aligned at the center.

If the bands are offset, the density of states will not overlap well, and the current will be reduced. If a gate electrode misaligns the two levels, the diminished current, at $T = 0$ K, will be

$$I_{0\,\text{K}} = 2q\frac{2\pi}{\hbar}|\mathbf{M}|^2\int_{-\infty}^{\infty}\left.\frac{dN(E-E_v)}{dE}\right|_{\text{v}}\left.\frac{dN(E-E_c)}{dE}\right|_c dE \tag{7}$$

where $T = 0$ K indicates a completely filled valence band dot and a completely empty conduction band dot. Because of the gate-induced offset between E_c and E_{v}, it could be that the region of common overlap will only occur in the band tails. Then, all the considerations of spectral tail shape will control the turnoff current characteristics. The predicted current–voltage curve for offset levels is shown in Fig. 6. The red curve shows the current–voltage behavior when the line shape is Lorentzian, while the blue curve is for the case of exponential line shapes. The current is normalized to $I_o = 2q(2\pi/\hbar)|M|^2(\tau/\pi\hbar)$, the Lorentzian peak current in (6), and the voltage difference on the horizontal axis is $\Delta V \equiv (E_c - E_{\text{v}})/q$.

If operating at $E_c - E_{\text{v}} < 4\ kT$, there will be partial occupation of both quantum dots and the current will be: $\Delta I = I_{0K}(q\Delta V/4kT)$, leading to a conductance $\text{G} \equiv \text{I}_{0\,\text{K}}(q/4kT)$.

As long as the spectral tails are exponential, $S(\Delta\omega) \sim \exp\{-2\Delta\omega\tau_p\}$, converting from frequency to voltage, and fall off as $dN/dE|_c \sim \exp\{-2q\Delta V\tau_p/\hbar\} \sim \exp\{-\Delta V/V_o\}$, the conductance tail will also fall exponentially, with the voltage swing $\equiv 2.303V_o \equiv (2.303\hbar/(2q\tau_p)) =$ 6 mV/decade for the value of τ_p specified in the caption of Fig. 6.

V. ON-STATE CONDUCTANCE LIMIT

In [72] and [73], it was shown that the matrix element $|\mathbf{M}|$ coupling the two quantum dots cannot be made arbitrarily large. $|\mathbf{M}|$ must be smaller than the damping linewidth, $|\mathbf{M}| < \hbar/4\tau$. If $|\mathbf{M}|$ were any larger, strong coupling between the two dots would occur. Under strong coupling, the electron would oscillate back and forth between quantum dots, and Lorentzian line shapes could return, making it impossible to turn the device off. Inserting $|\mathbf{M}| = \hbar/4\tau$ into Fermi's golden rule, the maximum tunneling current from (6) becomes $\sim q/4\tau$, which leads to tFET conductance, $\text{G}_{\text{tFET}} \equiv (q/4\tau)(q/4kT)$. Unfortunately, this is four times less than $\text{G}_{\text{contact}}$.

In effect, the operating tFET consists of three resistors in series, the two contact resistors on either side and the central tunnel resistor that is at least four times larger resistance. At best, the conductance of the device would be one-sixth of the contact conductance, which is itself limited by the quantum of conductance $2q^2/h$. To drive the wire capacitance rapidly enough, many such quantum dot tFETs would be required to operate in parallel.

Table 1 Summary of Formulas Connecting the tFET Electrical Properties With the Quantum Mechanical Parameters of the Device.

Quantities	Formula
(a) Single-channel wire--wire conductance vs. transmission probability	$G_{0K,wire-wire} = \frac{2q^2}{h}\mathrm{Tr}_{wire\text{-}wire}$
(b) Quantum-dot lifetime broadening due to wire tunneling	$\frac{\hbar}{\tau} = \frac{1}{\pi} E_z \mathrm{Tr}_{contact} = \frac{2\pi}{\hbar}\lvert X\rvert^2 \frac{2\tau_p}{\pi\hbar}$
(c) Dot-wire current at T=0K	$I_{0K} = q/\tau$
(d) Multi-channel conductance at finite temperature	$G(T) = G_{0K}(f_1 - f_2) \approx G_{0K}\left(\frac{q\Delta V}{4kT}\right), q\Delta V < 4kT$
(e) Multi-channel finite temperature conductance versus low temp current	$G(T) = I_{0K}\left(\frac{q}{4kT}\right), \quad q\Delta V < 4kT$
(f) Dot-wire conductance versus quantum dot lifetime	$G_{dot-wire} = \frac{q}{\tau} \times \frac{q}{4kT}$
(g) Peak value of the broadened quantum dot density of states	$\left.\frac{dN}{dE}\right\rvert_{dot-peak} = \frac{2\tau}{\pi\hbar}$
(h) Slope of the exponential tail of the broadened quantum dot density of states	$\omega_o = \frac{E_{narrow-band\ width}}{2} = \frac{\hbar}{2\tau_p}$
(i) Dot-dot matrix element versus dot-dot transmission probability	$\lvert\mathbf{M}\rvert=(1/\pi)\sqrt{(E_{z1}E_{z2}\mathrm{Tr})}$
(j) Dot-dot current at T=0K versus the convolved density of states	$I_{0K} = 2q\frac{2\pi}{\hbar}\lvert\mathbf{M}\rvert^2 \int_{-\infty}^{\infty} \left.\frac{dN(E-E_v)}{dE}\right\rvert_v \left.\frac{dN(E-E_c)}{dE}\right\rvert_c (f_v - f_c)dE$
(k) Dot-dot peak conductance versus dot-dot quantum transmission probability (Tr)	$G_{0K,dot-dot} = \frac{2q^2}{h}\frac{\mathrm{Tr}}{\mathrm{Tr}_{contact}^2}$
(l) Dot-dot conductance versus dot-dot quantum transmission probability (Tr), dN/dx is dN/dE normalized to its peak value (and hence dimensionless)	$G_{0K,dot-dot} = \frac{2q^2}{h}\frac{\mathrm{Tr}}{\mathrm{Tr}_{contact}^2}\left.\frac{dN(x-x_v)}{dx}\right\rvert_v \left.\frac{dN(x-x_c)}{dx}\right\rvert_c$
(m) Subthreshold slope (SS) versus narrow-band wire narrow band bandwidth	$SS = \frac{2.303E_{narrow-band\ width}}{2q} = \frac{2.303\hbar}{2q\tau_p}$
(n) Inter-dot conductance at strong coupling threshold versus quantum dot lifetime	$G_{dot-dot} = \frac{q}{4\tau}\frac{q}{4kT} = \frac{G_{dot-wire}}{4}$
(o) Effective circuit of the Double Quantum Dot tFET	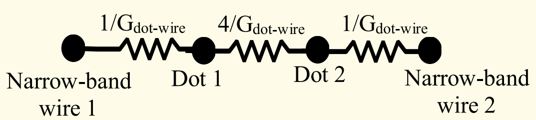

Agarwal and Yablonovitch [72], [73] also provide a useful estimate of the tunneling matrix element $|\mathbf{M}| = E_z\sqrt{\ }\mathrm{Tr}$, where E_z is the kinetic energy of ground state of the quantum dot, and Tr is the tunneling transmission probability. This formula can connect transmission probability to meaningful currents and voltages from Fermi's golden rule, recognizing that Tr is always <1.

The mathematical relationships among dot lifetime τ, tunnel transmission probability Tr, quantum confinement energy E_z, currents, and conductances are summarized in Table 1.

VI. CONCLUSION

To achieve a very steep slope in tFET response, many requirements must be fulfilled. Gate efficiency must be good. Defect-level concentration producing parasitic leakage must be very low. In addition, the energy levels must themselves be very sharp. The usual assumption of Lorentzian spectral broadening would not provide sufficient ON/OFF ratio to satisfy system needs. A correct use of Fermi's golden rule provides a mechanism for exponentially falling spectral tails, as required for a steep response. This demands that a narrowband, heavy effective mass, wire should mediate between the tunneling energy levels and the external metallic contacts. There are many additional requirements, including the need for the tunneling matrix element $|\mathbf{M}|$ to be reduced such that the system does not enter strong coupling but large enough to provide the maximum conductance.

In this paper, we have shown that exponential spectral tails can arise naturally as part of lifetime broadening, from the initial parabolic decay of population as provided by the more complete form of Fermi's golden rule given here. In turn, exponential spectral tails justify the concept of exponential steepness or voltage swing, as had always been assumed in tFETs.

In this paper, we have only considered T_1 or population decay processes. There may be many other contributions to spectral broadening including T_2 processes which will further challenge tFET performance. ■

REFERENCES

[1] F. Urbach, "The long-wavelength edge of photographic sensitivity and of the electronic absorption of solids," *Phys. Rev.*, vol. 92, p. 1324, Dec. 1953.

[2] K. C. Kao and G. A. Hockham, "Dielectric-fibre surface waveguides for optical frequencies," *Proc. Inst. Elect. Eng.*, vol. 113, no. 7, pp. 1151–1158, 1966.

[3] Y. Pan, F. Inam, M. Zhang, and D. A. Drabold, "Atomistic origin of Urbach tails in amorphous silicon," *Phys. Rev. Lett.*, vol. 100, no. 20, May 2008, Art. no. 206403.

[4] J. Liebler and H. Haug, "Calculation of the Urbach tail absorption in a second-order cumulant expansion," *Europhys. Lett.*, vol. 14, no. 1, pp. 71–76, Jan. 1991.

[5] S. John, M. Y. Chou, M. H. Cohen, and C. M. Soukoulis, "Density of states for an electron in a correlated Gaussian random potential: Theory of the Urbach tail," *Phys. Rev. B, Condens. Matter*, vol. 37, no. 12, pp. 6963–6976, Apr. 1988.

[6] B. Sadigh, P. Erhart, D. Åberg, A. Trave, E. Schwegler, and J. Bude, "First-principles calculations of the Urbach tail in the optical absorption spectra of silica glass," *Phys. Rev. Lett.*, vol. 106, no. 2, Jan. 2011, Art. no. 027401.

[7] S. John, C. Soukoulis, M. H. Cohen, and E. N. Economou, "Theory of electron band tails and the Urbach optical-absorption edge," *Phys. Rev. Lett.*, vol. 57, no. 14, p. 1777, 1986.

[8] T. H. Keil, "Theory of the Urbach rule," *Phys. Rev.*, vol. 144, no. 2, pp. 582–587, Apr. 1966.

[9] J. D. Dow and D. Redfield, "Toward a unified theory of Urbach's rule and exponential absorption edges," *Phys. Rev. B, Condens. Matter*, vol. 5, no. 2, pp. 594–610, Jan. 1972.

[10] A. M. Ionescu and H. Riel, "Tunnel field-effect transistors as energy-efficient electronic switches," *Nature*, vol. 479, no. 7373, pp. 329–337, 2011.

[11] J. J. Quinn, G. Kawamoto, and B. D. McCombe, "Subband spectroscopy by surface channel tunneling," *Surf. Sci.*, vol. 73, pp. 190–196, May 1978.

[12] S. Banerjee, W. Richardson, J. Coleman, and A. Chatterjee, "A new three-terminal tunnel device," *IEEE Electron Device Lett.*, vol. EDL-8, no. 8, pp. 347–349, Aug. 1987.

[13] W. Hansch, C. Fink, J. Schulze, and I. Eisele, "A vertical MOS-gated Esaki tunneling transistor in silicon," *Thin Solid Films*, vol. 369, nos. 1–2, pp. 387–389, Jul. 2000.

[14] J. Koga and A. Toriumi, "Negative differential conductance in three-terminal silicon tunneling device," *Appl. Phys. Lett.*, vol. 69, no. 10, pp. 1435–1437, Sep. 1996.

[15] T. Baba, "Proposal for surface tunnel transistors," *Jpn. J. Appl. Phys.*, vol. 31, no. 4B, pp. L455–L457, Apr. 1992.

[16] W. M. Reddick and G. A. J. Amaratunga, "Silicon surface tunnel transistor," *Appl. Phys. Lett.*, vol. 67, no. 4, pp. 494–496, 1995.

[17] C. Aydin *et al.*, "Lateral interband tunneling transistor in silicon-on-insulator," *Appl. Phys. Lett.*, vol. 84, no. 10, pp. 1780–1782, Mar. 2004.

[18] S. Mookerjea, D. Mohata, T. Mayer, V. Narayanan, and S. Datta, "Temperature-dependent I–V Characteristics of a Vertical $In_{0.53}Ga_{0.47}As$ tunnel FET," *IEEE Electron Device Lett.*, vol. 31, no. 6, pp. 564–566, Jun. 2010.

[19] M. O. Li, D. Esseni, G. Snider, D. Jena, and H. G. Xing, "Single particle transport in two-dimensional heterojunction interlayer tunneling field effect transistor," *J. Appl. Phys.*, vol. 115, no. 7, 2014, Art. no. 074508.

[20] A. S. Verhulst, W. G. Vandenberghe, K. Maex, and G. Groeseneken, "Tunnel field-effect transistor without gate-drain overlap," *Appl. Phys. Lett.*, vol. 91, no. 5, Jul. 2007, Art. no. 053102.

[21] K. E. Moselund, H. Schmid, C. Bessire, M. T. Bjork, H. Ghoneim, and H. Riel, "InAs–Si nanowire heterojunction tunnel FETs," *IEEE Electron Device Lett.*, vol. 33, no. 10, pp. 1453–1455, Oct. 2012.

[22] K. E. Moselund *et al.*, "Comparison of VLS grown Si NW tunnel FETs with different gate stacks," in *Proc. Eur. Solid State Device Res. Conf.*, Athens, Greece, 2009, pp. 448–451.

[23] O. M. Nayfeh, C. N. Chleirigh, J. Hennessy, L. Gomez, J. L. Hoyt, and D. A. Antoniadis, "Design of tunneling field-effect transistors using strained-silicon/strained-germanium type-II staggered heterojunctions," *IEEE Electron Device Lett.*, vol. 29, no. 9, pp. 1074–1077, Sep. 2008.

[24] F. Mayer *et al.*, "Impact of SOI, $Si_{1-x}Ge_x$OI and GeOI substrates on CMOS compatible Tunnel FET performance," in *IEDM Tech. Dig.*, San Francisco, CA, USA, Dec. 2008, pp. 1–5.

[25] R. K. Ghosh and S. Mahapatra, "Monolayer transition metal dichalcogenide channel-based tunnel transistor," *IEEE J. Electron Devices Soc.*, vol. 1, no. 10, pp. 175–180, Oct. 2013.

[26] J. Knoch, "Optimizing tunnel FET performance—Impact of device structure, transistor dimensions and choice of material," in *Proc. Int. Symp. VLSI Technol., Syst., Appl.*, Hsinchu, Taiwan, 2009, pp. 45–46.

[27] I. A. Young, U. E. Avci, and D. H. Morris, "Tunneling field effect transistors: Device and circuit considerations for energy efficient logic opportunities," in *IEDM Tech. Dig.*, Washington, DC, USA, Dec. 2015, pp. 22.1.1–22.1.4.

[28] H. Carrillo-Nuñez, M. Luisier, and A. Schenk, "InAs-GaSb/Si heterojunction tunnel MOSFETs: An alternative to TFETs as energy-efficient switches?" in *IEDM Tech. Dig.*, Washington, DC, USA, Dec. 2015, pp. 34.6.1–34.6.4.

[29] A. Seabaugh *et al.*, "Steep subthreshold swing tunnel FETs: GaN/InN/GaN and transition metal dichalcogenide channels," in *IEDM Tech. Dig.*, Washington, DC, USA, Dec. 2015, pp. 35.6.1–35.6.4.

[30] C. Wu, R. Huang, Q. Huang, J. Wang, and Y. Wang, "Design guideline for complementary heterostructure tunnel FETs with steep slope and improved output behavior," *IEEE Electron Device Lett.*, vol. 37, no. 1, pp. 20–23, Jan. 2016.

[31] J. Franco *et al.*, "Intrinsic robustness of TFET subthreshold swing to interface and oxide traps: A comparative PBTI study of InGaAs TFETs and MOSFETs," *IEEE Electron Device Lett.*, vol. 37, no. 8, pp. 1055–1058, Aug. 2016.

[32] Z. Yang, "Tunnel field-effect transistor with an L-shaped gate," *IEEE Electron Device Lett.*, vol. 37, no. 7, pp. 839–842, Jul. 2016.

[33] C. Hu *et al.*, "Prospect of tunneling green transistor for 0.1V CMOS," in *IEDM Tech. Dig.*, San Francisco, CA, USA, Dec. 2010, pp. 16.1.1–16.1.4.

[34] A. C. Seabaugh and Q. Zhang, "Low-voltage tunnel transistors for beyond CMOS logic," *Proc. IEEE*, vol. 98, no. 12, pp. 2095–2110, Dec. 2010.

[35] E. Baravelli, E. Gnani, R. Grassi, A. Gnudi, S. Reggiani, and G. Baccarani, "Optimization of n- and p-type TFETs Integrated on the same $InAs/Al_xGa_{1x}Sb$ technology platform," *IEEE Trans. Electron Devices*, vol. 61, no. 1, pp. 178–185, Jan. 2014.

[36] R. Asra, M. Shrivastava, K. V. R. M. Murali, R. K. Pandey, H. Gossner, and V. R. Rao, "A tunnel fet for V_{DD} scaling below 0.6 V with a CMOS-comparable performance," *IEEE Trans. Electron Devices*, vol. 58, no. 7, pp. 1855–1863, Jul. 2011.

[37] P. Long, E. Wilson, J. Z. Huang, G. Klimeck, M. J. W. Rodwell, and M. Povolotskyi, "Design and simulation of GaSb/InAs 2D transmission-enhanced tunneling FETs," *IEEE Electron Device Lett.*, vol. 37, no. 1, pp. 107–110, Jan. 2016.

[38] J. Zhu *et al.*, "Design and simulation of a novel graded-channel heterojunction tunnel FET with high I_{ON}/I_{OFF} ratio and steep swing," *IEEE Electron Device Lett.*, vol. 38, no. 9, pp. 1200–1203, Sep. 2017.

[39] J. T. Smith, S. Das, and J. Appenzeller, "Broken-gap tunnel MOSFET: A constant-slope sub-60-mV/decade transistor," *IEEE Electron Device Lett.*, vol. 32, no. 10, pp. 1367–1369, Oct. 2011.

[40] H. Lee, J.-D. Park, and C. Shin, "Performance booster for vertical tunnel field-effect transistor: Field-enhanced high-κ layer," *IEEE Electron Device Lett.*, vol. 37, no. 11, pp. 1383–1386, Nov. 2016.

[41] H. Ilatikhameneh, T. A. Ameen, G. Klimeck, J. Appenzeller, and R. Rahman, "Dielectric engineered tunnel field-effect transistor," *IEEE Electron Device Lett.*, vol. 36, no. 10, pp. 1097–1100, Oct. 2015.

[42] J. Appenzeller, Y.-M. Lin, J. Knoch, and P. Avouris, "Band-to-band tunneling in carbon nanotube field-effect transistors," *Phys. Rev. Lett.*, vol. 93, no. 19, Nov. 2004, Art. no. 196805.

[43] L. Knoll *et al.*, "Inverters with strained Si nanowire complementary tunnel field-effect transistors," *IEEE Electron Device Lett.*, vol. 34, no. 6, pp. 813–815, Jun. 2013.

[44] Q. Huang *et al.*, "A novel Si tunnel FET with 36 mV/dec subthreshold slope based on junction depleted-modulation through striped gate configuration," in *IEDM Tech. Dig.*, San Francisco, CA, USA, Dec. 2012, pp. 8.5.1–8.5.4.

[45] R. Gandhi, Z. Chen, N. Singh, K. Banerjee, and S. Lee, "CMOS-compatible vertical-silicon-nanowire gate-all-around p-type tunneling FETs with

≤50-mV/decade subthreshold swing," *IEEE Electron Device Lett.*, vol. 32, no. 11, pp. 1504–1506, Nov. 2011.

[46] T. Krishnamohan, D. Kim, S. Raghunathan, and K. Saraswat, "Double-Gate Strained-Ge Heterostructure Tunneling FET (TFET) With record high drive currents and ≪60 mV/dec subthreshold slope," in *IEDM Tech. Dig.*, San Francisco, CA, USA, Dec. 2008, pp. 1–3.

[47] K. Jeon *et al.*, "Si tunnel transistors with a novel silicided source and 46 mV/dec swing," in *Proc. Symp. VLSI Technol.*, Honolulu, HI, USA, Jun. 2010, pp. 121–122.

[48] D. Sarkar *et al.*, "A subthermionic tunnel field-effect transistor with an atomically thin channel," *Nature*, vol. 526, pp. 91–95, Sep. 2015.

[49] E. A. Casu *et al.*, "Hybrid phase-change—Tunnel FET (PC-TFET) switch with subthreshold swing < 10 mV/decade and sub-0.1 body factor: Digital and analog benchmarking," in *IEDM Tech. Dig.*, San Francisco, CA, USA, Dec. 2016, pp. 19.3.1–19.3.4.

[50] E. Memisevic, J. Svensson, M. Hellenbrand, E. Lind, and L.-E. Wernersson, "Vertical InAs/GaAsSb/GaSb tunneling field-effect transistor on Si with $S = 48$ mV/decade and $I_{on} = 10$ μA/μm for $I_{off} = 1$ nA/μm at $V_{DS} = 0.3$ V," in *IEDM Tech. Dig.*, San Francisco, CA, USA, Dec. 2016, pp. 19.1.1–19.1.4.

[51] P. Zhang, J. Wan, A. Zaslavsky, and S. Cristoloveanu, "CMOS-compatible FDSOI bipolar-enhanced tunneling FET," in *Proc. IEEE SOI-3D-Subthreshold Microelectron. Technol. Unified Conf. (S3S)*, Rohnert Park, CA, USA, Oct. 2015, pp. 1–3.

[52] Y. Morita *et al.*, "Experimental realization of complementary p- and n-tunnel FinFETs with subthreshold slopes of less than 60 mV/decade and very low (pA/μm) off-current on a Si CMOS platform," in *IEDM Tech. Dig.*, San Francisco, CA, USA, Dec. 2014, pp. 9.7.1–9.7.4.

[53] A. Saeidi *et al.*, "Negative capacitance as performance booster for tunnel FETs and MOSFETs: An experimental study," *IEEE Electron Device Lett.*, vol. 38, no. 10, pp. 1485–1488, Oct. 2017.

[54] X. Zhao, A. Vardi, and J. A. del Alamo, "Sub-thermal subthreshold characteristics in top-down InGaAs/InAs heterojunction vertical nanowire tunnel FETs," *IEEE Electron Device Lett.*, vol. 38, no. 7, pp. 855–858, Jul. 2017.

[55] E. Memisevic, J. Svensson, E. Lind, and L.-E. Wernersson, "Vertical nanowire TFETs with channel diameter down to 10 nm and Point S_{MIN} of 35 mV/decade," *IEEE Electron Device Lett.*, vol. 39, no. 7, pp. 1089–1091, Jul. 2018.

[56] A. Saeidi *et al.*, "Near hysteresis-free negative capacitance InGaAs tunnel FETs with enhanced digital and analog figures of merit below V_{DD}=400 mV," in *IEDM Tech. Dig.*, San Francisco, CA, USA, Dec. 2018, pp. 13.4.1–13.4.4.

[57] B. Rajamohanan *et al.*, "0.5 V supply voltage operation of $In_{0.65}Ga_{0.35}As/GaAs_{0.4}Sb_{0.6}$ tunnel FET," *IEEE Electron Device Lett.*, vol. 36, no. 1, pp. 20–22, Jan. 2015.

[58] H. Zhang, W. Cao, J. Kang, and K. Banerjee, "Effect of band-tails on the subthreshold performance of 2D tunnel-FETs," in *IEDM Tech. Dig.*, San Francisco, CA, USA, Dec. 2016, pp. 30.3.1–30.3.4.

[59] E. Memisevic, E. Lind, M. Hellenbrand, J. Svensson, and L.-E. Wernersson, "Impact of band-tails on the subthreshold swing of III-V tunnel field-effect transistor," *IEEE Electron Device Lett.*, vol. 38, no. 12, pp. 1661–1664, Dec. 2017.

[60] S. Agarwal, J. T. Teherani, J. L. Hoyt, D. A. Antoniadis, and E. Yablonovitch, "Engineering the electron–hole bilayer tunneling field-effect transistor," *IEEE Trans. Electron Devices*, vol. 61, no. 5, pp. 1599–1606, May 2014.

[61] J. L. Padilla, F. Gamiz, and A. Godoy, "A simple approach to quantum confinement in tunneling field-effect transistors," *IEEE Electron Device Lett.*, vol. 33, no. 10, pp. 1342–1344, Oct. 2012.

[62] K. Boucart and A. M. Ionescu, "Double-gate tunnel FET with high-κ gate dielectric," *IEEE Trans. Electron Devices*, vol. 54, no. 7, pp. 1725–1733, Jul. 2007.

[63] A. M. Walke *et al.*, "Fabrication and analysis of a $Si/Si_{0.55}Ge_{0.45}$ heterojunction line tunnel FET," *IEEE Trans. Electron Devices*, vol. 61, no. 3, pp. 707–715, Mar. 2014.

[64] S. Cristoloveanu, J. Wan, and A. Zaslavsky, "A review of sharp-switching devices for ultra-low power applications," *IEEE J. Electron Devices Soc.*, vol. 4, no. 5, pp. 215–226, Sep. 2016.

[65] A. W. Dey *et al.*, "High-current GaSb/InAs(Sb) nanowire tunnel field-effect transistors," *IEEE Electron Device Lett.*, vol. 34, no. 2, pp. 211–213, Feb. 2013.

[66] J. Knoch, S. Mantl, and J. Appenzeller, "Impact of the dimensionality on the performance of tunneling FETs: Bulk versus one-dimensional devices," *Solid-State Electron.*, vol. 51, no. 4, pp. 572–578, Apr. 2007.

[67] C. Cohen-Tannoudji, J. Dupont-Roc, and G. Grynberg, "Discrete state coupled to a finite-width continuum: From the Weisskopf–Wigner exponential decay to the Rabi oscillation," in *Atom–Photon Interactions: Basic Process and Appilcations*. New York, NY, USA: Wiley, 1992, pp. 250–251.

[68] S. Agarwal and E. Yablonovitch, "Fundamental conductance ÷ voltage limit in low voltage tunnel switches," *IEEE Electron Device Lett.*, vol. 35, no. 10, pp. 1061–1062, Oct. 2014.

[69] S. Agarwal and E. Yablonovitch. (Sep. 2011). "Pronounced effect of pn-junction dimensionality on tunnel switch threshold shape." [Online]. Available: https://arxiv.org/abs/1109.0096

[70] S. Agarwal and E. Yablonovitch, "Designing a low-voltage, high-current tunneling transistor," in *CMOS and Beyond: Logic Switches for Terascale Integrated Circuits*, T.-J. K. Liu and K. Kuhn, Eds. Cambridge, U.K.: Cambridge Univ. Press, 2015, pp. 79–116.

ABOUT THE AUTHORS

Sri Krishna Vadlamani (Member, IEEE) received the B.Tech. degree in electrical engineering from IIT Bombay, Mumbai, India, in 2016. He is currently working toward the Ph.D. degree in electrical engineering and computer sciences at the University of California at Berkeley, Berkeley, CA, USA.

In 2015, he was an Intern with the Theory and Simulation of Materials Group, École Polytechnique Fédérale de Lausanne (EPFL), Lausanne, Switzerland. His current research interests include quantum physics, optics, and the intersection of physics and computing.

Sapan Agarwal (Member, IEEE) received the Ph.D. degree in electrical engineering from the University of California at Berkeley, Berkeley, CA, USA, in 2012, under the supervision of Prof. E. Yablonovitch.

He is currently a Senior Member of Technical Staff with the Sandia National Laboratories, Albuquerque, NM, USA. He is also with the IEEE International Roadmap for Devices and Systems to map out future computing architectures and devices. He has invented several new semiconductor device concepts including new low-power transistors, artificial analog synapses, and wide-bandgap LEDs. His current research interests include explainable machine learning, in memory computing accelerators, neuromorphic hardware, semiconductor devices, and photonic devices.

David T. Limmer received the bachelor's degree in chemical engineering from the New Mexico Institute of Mining and Technology, Socorro, NM, USA, in 2008, and the Ph.D. degree in theoretical chemistry from the University of California at Berkeley, Berkeley, CA, USA, in 2013.

From 2013 to 2016, he was a Fellow of the Princeton Center for Theoretical Science, Princeton University, Princeton, NJ, USA. In 2016, he joined the Faculty of the University of California at Berkeley, where he holds various faculty scientist positions with the Chemistry and Materials Science Divisions, Lawrence Berkeley National Laboratory. He is a member of the Kavli Energy NanoSciences Institute, Berkeley, CA, USA. At the University of California at Berkeley, his research group endeavors to advance theoretical descriptions of complex, condensed phase materials, especially in instances where equilibrium ideas do not apply. His current research interests include the emergent behavior of systems undergoing simple chemical dynamics in complex environments, the response of nanoscale systems driven far from equilibrium, and the solid–electrolyte interfaces relevant to basic energy science.

Dr. Limmer is a Lindau and Scialog Fellow. He held the Chevron Chair. He was a recipient of a Heising-Simons Fellowship.

Steven G. Louie received the Ph.D. degree in physics from the University of California at Berkeley (UC Berkeley), Berkeley, CA, USA, in 1976.

After having worked at the IBM Watson Research Center, Bell Labs, and UPenn, he joined the UC Berkeley faculty in 1980, where he is currently a Professor of physics and concurrently, a Faculty Senior Scientist at the Lawrence Berkeley National Lab. His research spans a broad spectrum of topics in theoretical condensed matter physics and nanoscience. He is known for his ground-breaking work on the ab initio GW method and for his seminal work on surfaces and interfaces, nanostructures, and reduced-dimensional systems.

Prof. Louie is a member of the National Academy of Sciences, the American Academy of Arts & Sciences, and the Academia Sinica (Taiwan), as well as a Fellow of the American Physical Society (APS), the American Association for the Advancement of Science, and the Materials Research Society. Among his many honors, he is a recipient of the APS Aneesur Rahman Prize for Computational Physics, the APS Davisson-Germer Prize in Surface Physics, the Materials Theory Award of the Materials Research Society, the Foresight Institute Richard P. Feynman Prize in Nanotechnology, the U.S. Department of Energy Award for Sustained Outstanding Research in Solid State Physics, as well as the Jubilee Professor of the Chalmers University of Technology in Sweden, and the H. C. ÃŸrsted Lecturer of the Technical University of Denmark.

Felix R. Fischer was born in Heidelberg, Germany, in 1980. He received the Ph.D. degree in chemistry from the Swiss Federal Institute of Technology, Zürich, Switzerland, in 2008.

He was a Postdoctoral Researcher at Columbia University, New York, NY, USA. In 2011, he was an Assistant Professor at the University of California at Berkeley, Berkeley, CA, USA, where he has been an Associate Professor with the Department of Chemistry since 2017. His current research interests include carbon-based nanotechnology, covalent surface self-assembly, and advanced functional materials for electronic device applications.

Dr. Fischer was a recipient of the Packard Fellowship for Science and Engineering in 2013, the DOE Early Career Award in 2013, the NSF Early Career Award in 2015, the Carl–Duisberg Prize of the German Chemical Society in 2016, and the *Journal of Physical Organic Chemistry* Award for Early Excellence in 2017.

Eli Yablonovitch (Fellow, IEEE) received the Ph.D. degree in applied physics from Harvard University, Cambridge, MA, USA, in 1972.

He is currently the Director of the NSF Center for Energy Efficient Electronics Science (E^3S), a multi-University Center headquartered at Berkeley, a Senior Faculty Scientist at the Lawrence Berkeley National Laboratory, and the James & Katherine Lau Engineering Chair Professor in electrical engineering and computer sciences at the University of California at Berkeley, Berkeley, CA, USA. He introduced the idea that strained semiconductor lasers could have superior performance due to reduced valence band (hole) effective mass. With almost every human interaction with the internet, optical telecommunication occurs by strained semiconductor lasers. In his photovoltaic research, he introduced the 4(n squared) (*Yablonovitch Limit*) light-trapping factor, in worldwide use for almost all commercial solar panels. Based on his mantra that a great solar cell also needs to be a great LED, his startup company Alta Devices Inc., Sunnyvale, CA, USA, holds the world record for solar cell efficiency, now 29.1% at 1 sun. He is regarded as a Father of the Photonic BandGap concept, and he coined the term Photonic Crystal. The geometrical structure of the first experimentally realized Photonic bandgap is sometimes called *Yablonovite*. His startup company Ethertronics Inc., San Diego, CA, USA, shipped over two billion cellphone antennas.

Dr. Yablonovitch has been elected to the NAE, NAS, NAI, AmAcArS, and as a Foreign Member, U.K. Royal Society. He was a recipient of the OSA Ives/Quinn Medal, the Benjamin Franklin Medal, the IEEE Edison Medal, the Buckley Prize of the American Physical Society, and the Isaac Newton Medal of the U.K. Institute of Physics.